(SPLIT-)QUATERNION AND (SPLIT-)OCTONION DYNAMICS IN DISCRETE-TIME RECURRENT FRENET FRAMES

BERND BINDER

Quanics, Germany

Accepted for Publication by the Journal of Discontinuity, Nonlinearity, and Complexity

Abstract. We consider and apply a multidimensional discrete-time delay autonomous third order non-linear vector difference equation system, where the orthogonal change after two reflections is given by a vector cross product leading to spinor rotations $X_i - X_{i-2} = -X_{i-1} \times F_i\left(X_{i-1}, X_{i-2}, X_{i-3}\right) \in \mathbb{R}^3$ or $\in \mathbb{R}^7$, where the symmetry invariant $C = X_i \cdot X_{i-1} = X_{i-1} \cdot X_{i-2} = ...$ allows at every step for a polar charge generating sign flip including expansion/contraction by a scalar factor. Using the Frenet frame approach defining orthogonal co-moving components with torsion and curvature parameter, both, the orthogonal frame and the change of the frame are represented by the three position memory terms recurrently. The necessary cross and dot vector product (split-)algebra is encoded in variable multiplication tables in $3d$ and $7d$. We discuss two special F_i types showing stable point densities, which are drifting limit cycles with sub-cycles, where the resulting smooth orbital spinor dynamics shows discrete atomic-type orbital eigenstates or local waves with characteristic numbers, non-local reflection, instability, hysteresis, interaction, helical emissions, and transition to chaos. Limit cycle modular arithmetic with equivalence classes characterizes the resulting point groups, rings, or N_j-gons, where sub-cycles appear on three levels with a total limit cycle length given by the product of the three sub-cycle lengths.

1. Introduction

With memory or time-delay recurrent functions, we get a rich variety of discontinuous, nonlinear, and complex phenomena, where we can have multiple bifurcations, limit cycles or periodic solutions and co-existence of trivial attractors (fixed points or limit cycles) and strange (chaotic) attractors. In this paper we will consider discrete-time equations with algebraic operations and corresponding symmetries typical for spinors in higher dimensional Euclidean spaces $\mathbb{R}^n$, where we focus on $n = 3$ and $n = 7$. Initially, we started in two Euclidean dimensions or on spherical surfaces [1] producing some chaotic and regular pattern by discrete-time Rotation-Translation-Reflection chaotic algorithms inspired by Skiadas in 2009 [2]. We often wondered, how both, symmetry and regular non-linear flow-type structures can arise out of a time-discrete chaotic dynamics. In 2022 we switched to $3d$ allowing for rotations and helical paths with variable direction, where the $3d$ cross product rotates the rotator axis and provides for the orthogonal or tangential unit translation. The reflection operation generates two opposite "charged" density pairs leading to pairs of limit cycles, where we get small shifts producing smooth orbital waves with regular or chaotic spin dynamics on curved surfaces [3,4]. Here the reflection as a permanent sign-flip shows an alternating two-period even/odd tuple symmetry, a "ping-pong" responsible for small non-linear geometric shifts [1]. So we have both, a long-range non-local jump in the first step and in total a small local shift or double reflection after jumping back in the second step. This way we found orbital wave function pairs with eigenstates resembling charged quantum states, where we could stimulate spin-transitions and a lot of non-linear dynamics like decays or spontaneous phase changes showing hysteresis and pairing effects.

E-mail address: binder@quanics.com.

Date: July 26, 2024.

2010 *Mathematics Subject Classification.* 60-J74, 57-R25, 35-A04.

Key words and phrases. Discrete, Frenet, Octonion, Quaternion, Quantum, Spinor, Orbital, Limit Cycle, Cross Product, Sphenic.

TABLE 1. Normed algebras and Lorentz group isomorphisms.

$x = n + 1$	x-dimensional Species	Division Algebras	Split Algebras
1	Real numbers	$SO(2,1) \simeq SL(2,\mathbb{R})$	$SO(2,1) \simeq SL(2,\mathbb{R}')$
2	Complex numbers	$SO(3,1) \simeq SL(2,\mathbb{C})$	$SO(2,2) \simeq SL(2,\mathbb{C}')$
4	Quaternions	$SO(5,1) \simeq SL(2,\mathbb{H})$	$SO(3,3) \simeq SL(2,\mathbb{H}')$
8	Octonions	$SO(9,1) \simeq SL(2,\mathbb{O})$	$SO(5,5) \simeq SL(2,\mathbb{O}')$

In our original concept the rotation strength was proportional to the inverse power-law of the radial distance [3]. Recently, we switched under SO(3) from the Euler angle rotation function to the vector cross product orthogonal rotation [4]. This new concept is motivated by the following arguments:

(1) On the discrete path in $\mathbb{R}^3$ a small orthogonal tangential shift leads to a small rotation of the two vectors orthogonal to the tangent vector and orthogonal to each other.
(2) These three orthogonal vectors can define a co-moving local orthogonal frame, which can be split by a cross product algebra into 3 orthogonal parts given by the tangential, normal, and binormal unit vectors constituting a Frenet frame.
(3) Applying the cross product algebra we don't need transcendental functions and a rotation matrix to perform rotations, which provides for a considerable computational performance boost in simulations.
(4) A special kind of orthogonality in the discrete sequence will lead to symmetry invariants supporting stability of limit cycle path at the edge to chaos.
(5) The cross product algebra well known in $3d$ can describe quaternion spin dynamics (classical physics) and can be extended to $7d$, where we have some famous octonion spinor relations well known in relativistic quantum physics.

2. Cross and Dot Product Algebra

The cross product of two vectors gives a third vector that is perpendicular to the two input vectors, where the symbol "$\times$" will always denote a vector cross and "$\cdot$" a vector dot product. For example, if we let $X = (x_1, x_2, x_3)$ and $Y = (y_1, y_2, y_3)$, we have $X \times Y := (x_2y_3 - x_3y_2, x_3y_1 - x_1y_3, x_1y_2 - x_2y_1)$ and $X \cdot Y := x_1y_1 + x_2y_2 + x_3y_3$. If e_i are three orthogonal unit vectors in $\mathbb{R}^3$ we have $e_1 \times e_2 = e_3$, $e_2 \times e_3 = e_1$, and $e_1 \times e_3 = -e_2$ determining the right-hand-rule of the cross product. If M is a square matrix then $|M|$ denotes the determinant of M with

$$(X \times Y) = \begin{vmatrix} e_1 & e_2 & e_3 \\ x_1 & x_2 & x_3 \\ y_1 & y_2 & y_3 \end{vmatrix}.$$

Let $X \neq 0$, $Y \neq 0$, $\widetilde{X}$, and $\widetilde{Y}$ be vectors in $\mathbb{R}^3$ and let a, b, c, and d be real numbers and θ the angle formed by the two input vectors X and Y, some of the basic properties of the dot and cross products are:

(1) $X \cdot (X \times Y) = 0$ and $Y \cdot (X \times Y) = 0$ (orthogonality)
(2) $(X \times Y) \cdot (X \times Y) + (X \cdot Y)^2 = (X \cdot X)(Y \cdot Y)$ (Pythagorean)
(3) $\frac{(X \cdot Y)}{\sqrt{(X \cdot X)(Y \cdot Y)}} = \cos\theta$, $\frac{||(X \times Y)||}{\sqrt{(X \cdot X)(Y \cdot Y)}} = \sin\theta$ (transcendental mapping)
(4) $(aX + b\widetilde{X}) \times (cY + d\widetilde{Y}) = ac(X \times Y) + ad(X \times \widetilde{Y}) + bc(\widetilde{X} \times Y) + bd(\widetilde{X} \times \widetilde{Y})$ (bilinearity)

We can extend the basic recurrent nonlinear algebraic system from $\mathbb{R}^3$ to $\mathbb{R}^7$, since the standard cross products of normed division and split-algebras can exist in $\mathbb{R}^n$ if and only if $n = 0$, 1, 3 or 7, see Hurwitz in 1898 [5] and Hasebe [6] with Hopf map relations and Lorentz group isomorphisms summarized in Table 1. So our cross products exist on $\mathbb{R}^n$ for $n = 3$ (quaternion algebra) and can be extended to $n = 7$ (octonion algebra) with orthonormal basis $e_1, e_2 \ldots e_n$, where for any $i \neq j$ there is a k with $e_i \times e_j = ae_k$ for $a = 1$ or -1.

Since we are dealing with rotating rotation axes and spinors we have an eye on emerging symmetries due to orthogonality. The orthogonality property (1.) will be very important regarding the discrete evolution

of the co-moving Frenet frame according to a symmetry invariant. The quaternion and octonion algebra defining generalized cross and dot products of two vectors can be encoded in general matrix multiplication tables, see chapter 4.

3. Discrete Space Curves

Discrete space curves are important in discrete differential geometry. Our focus is on *discrete spaces* with the map

$$X : \mathbb{Z} \to \mathbb{R}^3 \text{ or } \mathbb{R}^7, \quad (i \mapsto X_i), \tag{1}$$

where three successive vector points X_{i-2}, X_{i-1}, X_i are separated by discrete "jumps", ordered in discrete time $t_{i+1} = t_i + \Delta t_i$, and are not located on a straight line. In the following subsections we will relate these three memory vectors to the orthogonal vectors in the Frenet frame.

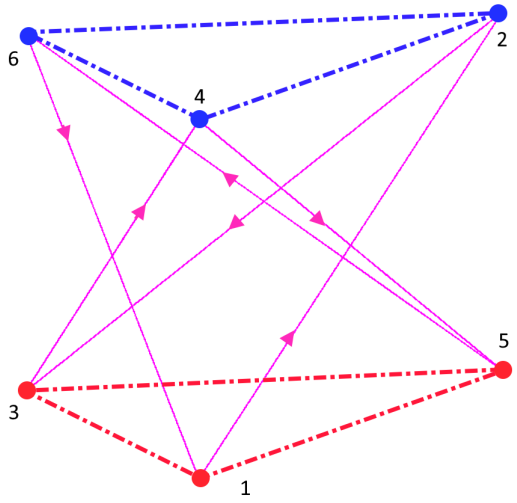

Figure 1. Projection of a triangular quaternion limit cycle pair (blue, red) system, where we have F_i type 2, $m = 6$ limit cycle connections, see Table 4. Note, that the red and blue edge points show a reflection mirror symmetry.

3.1. **Limit Cycles with Small Shifts.** A discrete space curve X according to Eq.(1) is said to be *closed* of length m if $X_{i\pm m} = X_i$ for any $m \in \mathbb{Z}$, see Fig.1 with $m = 6$ or Fig.3 with $m = 470$. This is the closed loop or return condition, where the shift $\varepsilon_i = |X_i - X_{i\pm m}| > 0$ or distance after one cyclic loop in real simulations can be made infinitesimally small. In a computer simulation some hundreds of operations within a typical display refresh time unit (20 ... 60 Hz) already show a smooth limit cycle kinematics.

3.2. **Governing Equations.** Recently we pointed to symmetries in a discrete-time delay autonomous third order non-linear difference equation vector system (three position vector memory terms) using a normed cross product algebra presented in [4], where the cross product of the last local vector X_{i-1} with a vector function $F_i\left(X_{i-1}, X_{i-2}, X_{i-3}\right)$ based on the last 3 memorized points provides for an orthogonal rotational change $X_i - X_{i-2}$

$$X_i - X_{i-2} = -X_{i-1} \times F_i\left(X_{i-1}, X_{i-2}, X_{i-3}\right) \in \mathbb{R}^3 \text{ or } \in \mathbb{R}^7, \tag{2}$$

see the simplified discrete evolution shown in Fig.2. The orthogonal change and rotational shifts after two reflections is given by a vector cross product, where the reflection operations are given by

$$X_{i-3} = -X_{i-2}/c_4, \; X_{i-2} = -X_{i-1}c_4, \; X_{i-1} = -X_i/c_4. \tag{3}$$

Here symmetry allows at every step for a memory reflection sign flip including expansion/contraction by a scalar factor $c_4 > 0$. In most cases we set $c_4 = 1$ in Eq.(3).

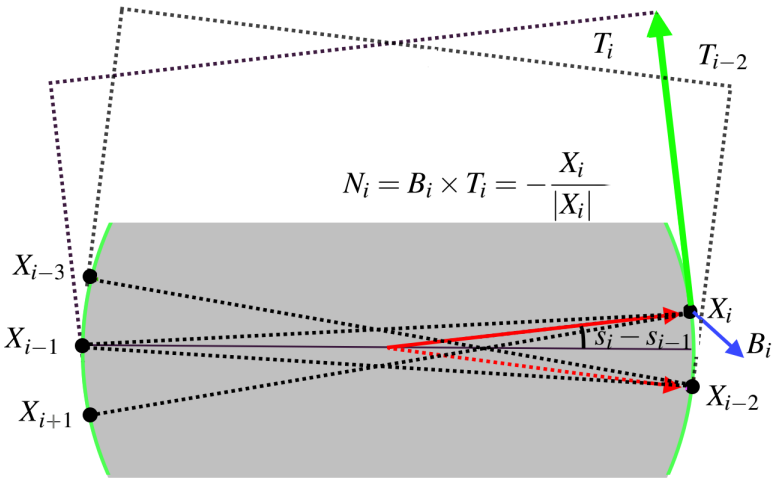

FIGURE 2. The three orthogonal Frenet frame vectors T_i, N_i, B_i related by a cross product based on the three memorized points $X_{i-3}, X_{i-2}, X_{i-1}$ in a simplified circular osculating situation, where the odd points are on the opposite site of even points due to reflection for $c_4 = 1$.

3.3. **Symmetry and the Frenet Frame.** According to Noethers Theorem, symmetry exhibits an observable quantity that is conserved. The reflection relations shown in Eq.(3) provide for a symmetry that can be seen in spatial separated co-orbiting mirror-image density pattern, a kind of pattern-antipattern symmetry, which are two spatially separated counter sets appearing as even/odd tuples (even/odd index i) [1] defining opposite "charge" sets based on the alternating "jumps". The orthogonality and symmetries within the three subsequent memory terms carries the information of an orthogonal frame and provide for resilience and stability. In Eq.(2) the cross product $X_{i-1} \times F_i$ equal to the tangential difference $X_i - X_{i-2}$ is orthogonal to the intermediate point X_{i-1} with invariant C

$$C = X_i \cdot X_{i-1} = X_{i-1} \cdot X_{i-2} = ..., \ (X_{i-2} - X_i) \cdot X_{i-1} = 0, \tag{4}$$

where C can be related to a rotation angle $s_i - s_{i-1}$

$$C = -|X_i|\,|X_{i-1}| \cos(s_i - s_{i-1}) = -|X_{i-1}|\,|X_{i-2}| \cos(s_{i-1} - s_{i-2}) = ... , \tag{5}$$

and $C < 0$ for $c_4 > 0$. In this context we have

$$X_{i-1} \cdot (X_i + X_{i-2}) = 2C \ . \tag{6}$$

This allows to use a discrete Frenet frame apparatus defining orthogonal co-moving components (tangential, normal, binormal) with torsion and curvature parameter, where both, the orthogonal frame and the change of the frame are represented by the three position memory terms recurrently. In this work we derive two types of vector functions F_i. Type 1 is directly based on the Frenet frame apparatus. Type 2 is a modification containing no unit vector normalization terms, but power-law distance dependent terms. In Fig.2 we see the discrete-time evolution of the four actual position vectors and three frame vectors T_i, B_i, and N_i. To get the geometric properties of the curves itself, the discrete Frenet-Serret formulas, see e.g. Hu, Lundgren, and Niem [7] or Blair and Konno [8], provide for an standard model of orthogonal frame vectors given by the so-called tangent T_i, normal N_i, and binormal B_i unit vectors in terms of each other. The frame vectors have unit length $|N_{i-1}| = |B_{i-1}| = |T_{i-1}| = 1$ and are orthogonalized by cross and dot product operations

$$N_i = B_i \times T_i \ . \tag{7}$$

First we note, that in a simple spherical symmetric situation the normal vector N_i points to the center of motion $N_i = -X_i/|X_i|$, which means that the coordinate center is equal to the reflection center and the normal vector is anti-parallel to the position vector, see Fig.2.

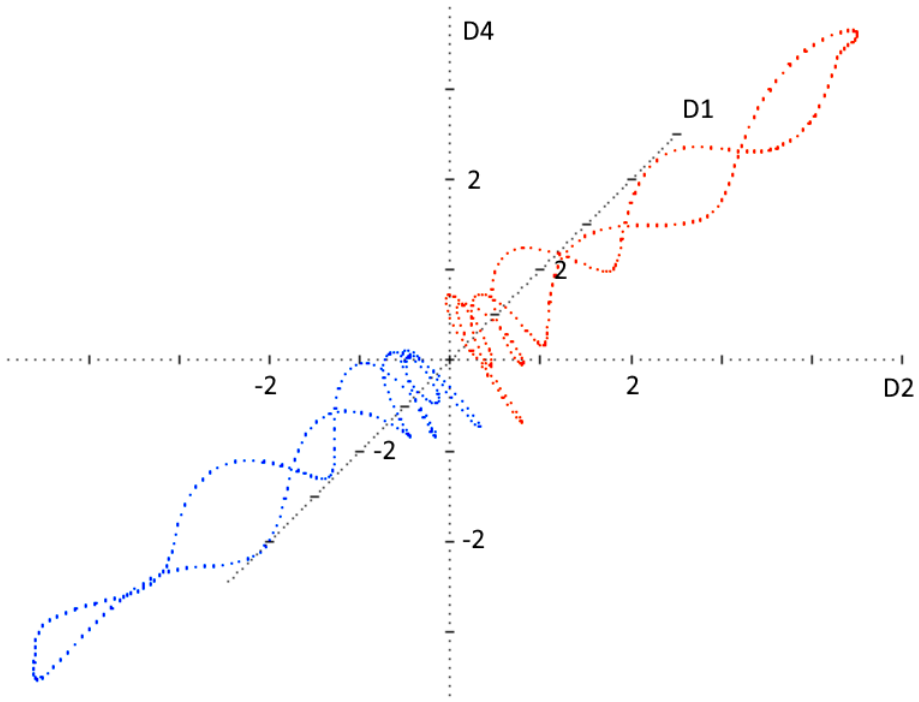

FIGURE 3. A type 1 quaternion sequence including reflection, where the odd points (blue) are on the left and the even points (red) on the right. The quaternion is "hosted" in an octonian, where the depicted three imaginary quaternion dimensions (D1, D2, D4) are a subset of the eight octonion dimensions (D0, ..., D7). The closed cycle has $m = 470$ points, $\tau \approx 0.01264$, $\kappa \approx 0.09656$, $C = \alpha = 1$.

3.4. **Type 1 Frenet frame vector function.** A co-moving frame can provide for kinematic properties like local orientation, velocity, acceleration, curvature, and torsion along the arc. Regarding the discrete change of the frame, in a limit cycle which is closed after m steps, the angular change or arc length difference after one loop is infinitesimally small with arbitrary slow rotation $s_{i-m} - s_i$ and can go to zero $\varepsilon = |X_i - X_{i\pm m}| \to 0$. In this case the fixed point drift is arbitrary smooth and can be a differential $\Delta s_{i,m} = s_{i-m} - s_i \to ds_{i,m}$. The change in the normal component after a closed loop with m steps and infinitesimal position change can be directly related to the continuous Frenet-Serret formula

$$\frac{N_{i-m} - N_i}{s_{i-m} - s_i} = \frac{\Delta N_{i,m}}{\Delta s_{i,m}} \to \frac{dN_{i,m}}{ds_{i,m}} = \tau_{i,m}\, B_{i,m} - \kappa_{i,m}\, T_{i,m}\ , \tag{8}$$

where $\kappa_{i,m}$ is the curvature and $\tau_{i,m}$ the torsion parameter in discrete time on a closed loop. Since $B_{i,m}$ and $T_{i,m}$ must be both orthogonal to $N_{i,m}$, the central requirement of orthogonal change in the Frenet continuous case can be written as

$$\frac{dN_{i,m}}{ds_{i,m}} \cdot N_{i,m} = 0. \tag{9}$$

With circular osculating symmetry on both sides (even/odd index) we have $|X_i| = |X_{i-2}|$, where with Eq.(4) the orthogonal change of the normal vector is related to a two step arc length $\Delta s_{i,2}$ by

$$\frac{\Delta N_{i,2}}{\Delta s_{i,2}} \cdot N_{i-1} = 0. \tag{10}$$

Now three normal vectors N_{i-3}, N_{i-2}, N_{i-1} define the actual orthogonal frame and will be used to construct the next normal vector N_i and frame and with symmetry invariant

$$\frac{N_i \cdot N_{i-1}}{\Delta s_{i,2}} = \frac{N_{i-1} \cdot N_{i-2}}{\Delta s_{i-1,2}} = ... = \frac{\cos(s_{i-1} - s_i)}{\Delta s_{i,2}} = -\frac{\cos(\Delta s_{i,2}/2)}{\Delta s_{i,2}}. \tag{11}$$

In terms of the position vector we have

$$\frac{\Delta N_{i,2}}{\Delta s_{i,2}} = \frac{N_{i-2} - N_i}{\Delta s_{i,2}} = \frac{1}{\Delta s_{i,2}} \left(\frac{X_i}{|X_i|} - \frac{X_{i-2}}{|X_{i-2}|} \right) = -\frac{\Delta X_{i,2}}{\alpha_i}, \tag{12}$$

where

$$\alpha_i = \Delta s_{i,2} \, |X_i| \tag{13}$$

relates the length of the position vector to the arc change of the normal vector as a constant orbital velocity. Within two steps including two reflections the Frenet-Serret equation Eq.(8) gives the normal vector change

$$\frac{\Delta N_{i,2}}{\Delta s_{i,2}} = \tau_{i-1} \frac{X_{i-1} \times X_{i-2}}{|X_{i-1} \times X_{i-2}|} - \kappa_{i-1} \frac{X_{i-1} \times X_{i-3}}{|X_{i-1} \times X_{i-3}|}, \tag{14}$$

where the binormal and tangential unit frame vectors are given by

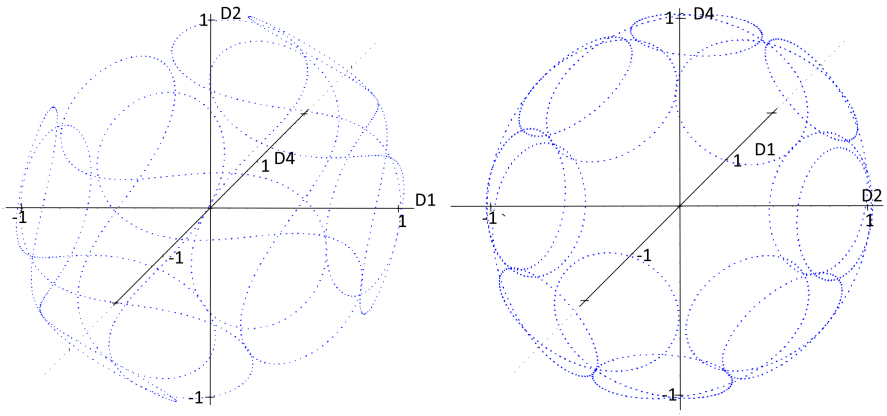

FIGURE 4. A highly regular type 1 quaternion pattern on a unit sphere with $C = 1$, it is a limit cycle (see Table 4) with $m = 3 \cdot 7 \cdot 59 = 1239$, $\kappa \approx 0.0073\pi \approx \tau/\sqrt{3}$, $c_4 = 1.0$.

$$B_i = c_B^{-1} X_{i-1} \times X_{i-2}, \; T_i = c_T^{-1} X_{i-1} \times X_{i-3}, \tag{15}$$

which are normalized by c_B and c_T

$$c_B = |X_{i-1} \times X_{i-2}|, \; c_T = |X_{i-1} \times X_{i-3}|. \tag{16}$$

With $\alpha_i \Delta N_{i,2} = \Delta s_{i,2} X_{i-1} \times F_i(...)$, Eq.(2), and Eqs.(12-16) we have

$$F_i \left(X_{i-1}, X_{i-2}, X_{i-3} \right) = \alpha_i \left[X_{i-2} c_B^{-1} \tau_{i-1} - X_{i-3} c_T^{-1} \kappa_{i-1} \right]. \tag{17}$$

As the central concept of this paper, both, the orthogonal frame and the change of the frame are represented by $F_i \left(X_{i-1}, X_{i-2}, X_{i-3} \right)$ in Eq.(17) with 3 position memory terms recurrently. Results based on Eq.(17) are shown in Fig.3 and Fig.4.

3.5. **Type 2 Orthogonal frame vector function.** In our computer experiments we have been looking for variants of F_i in the three-memory term Frenet concept and found

$$F_i\left(X_{i-1},X_{i-2},X_{i-3}\right)=\alpha_i\left[c_1\frac{X_{i-2}}{|X_{i-2}-X_{i-1}|^{p_1}}+c_2\frac{X_{i-3}}{|X_{i-3}-X_{i-1}|^{p_2}}\right]. \tag{18}$$

Note, that here we have a power-law distance dependence similar to the previous work of Skiadas [2]. The discrete two-step difference equation with the normal vector orthogonal to difference of successive vectors is is with Eqs.(2) and (18) given by

(19)

$$\Delta X_i=X_i-X_{i-2}=-X_{i-1}\times F_i\left(X_{i-1},X_{i-2},X_{i-3},...\right)=\alpha_i\left[c_1\frac{X_{i-1}\times X_{i-2}}{|X_{i-2}-X_{i-1}|^{p_1}}+c_2\frac{X_{i-1}\times X_{i-3}}{|X_{i-3}-X_{i-1}|^{p_2}}\right]$$

Default values for the exponents are $p_1=p_2=1$, since we get in this case a scale-invariant dynamics. Comparing Eq.(14) to Eq.(19) we have the standard bilinear normalization terms and get for Eq.(19) reflection-distance power-law dependent torsion and curvature functions

$$\tau_{i-1}=\frac{c_1c_B}{|X_{i-2}-X_{i-1}|^{p_1}}\ ,\kappa_{i-1}=\frac{c_2c_T}{|X_{i-3}-X_{i-1}|^{p_2}}\ . \tag{20}$$

The scalar control parameter can be related by

(21)

$$N_{i-1}=c_N^{-1}X_{i-1}=B_{i-1}\times T_{i-1}=c_B^{-1}c_T^{-1}(X_{i-1}\times X_{i-2})\times(X_{i-1}\times X_{i-3})=c_B^{-1}c_T^{-1}X_{i-1}\left(X_{i-1}\cdot(X_{i-2}\times X_{i-3})\right),$$

where we find the triple vector product or $3d$ polar sine

$$c_N^{-1}c_Bc_T=X_{i-1}\cdot(X_{i-2}\times X_{i-3})=-X_{i-2}\cdot(X_{i-3}\times X_{i-1})=-X_{i-3}\cdot(X_{i-1}\times X_{i-2}). \tag{22}$$

In contrast to the standard Frenet normalization we have with $p_1=p_2=1$ a scale-invariant distance dependent unit vector normalization in Eq.(19). Both variants show similar results in spherical symmetry, if we have $p_1=p_2=1$, $C=1$, and small angles $s_{i-2}-s_i$, see Fig.2, since in this case

$$|X_{i-1}\times X_{i-2}|\approx|X_{i-2}-X_{i-1}||X_{i-1}|,\ |X_{i-1}\times X_{i-3}|\approx|X_{i-3}-X_{i-1}||X_{i-2}|. \tag{23}$$

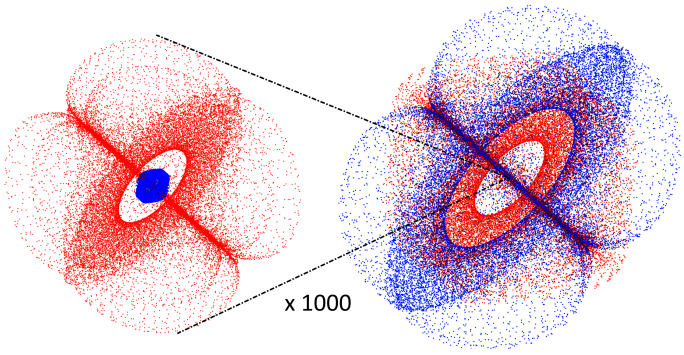

FIGURE 5. Two coupled type 2 quaternion systems with rotating orbital wave functions with coupling given by $\beta_{XY,i}=-\beta_{YX,i}$ showing atomic type structures with inner core and outer orbital states, where the core (on the left side) is very tiny. $c_1\approx-0.0073$, $c_2\approx0.02$, $c_3\approx-0.0073$, $c_4\approx7.5$, $p_1=p_2=1$, $p_3=2$, $C_X=C_Y=\alpha=1$, where the size difference is given by $c_4\neq1$.

3.6. **Coupled Systems.** An external coupling means, that the frame change is not only driven by the internal frame vectors, but also from external frame vectors introducing additional external vector shifts affecting curvature and torsion with an extended symmetry invariant. In this paper we will only consider examples of a mutual coupling between two systems. Coupling two systems X and Y having the same vector function F_i, the coupling from the Y-system to the X-system could be given by

$$X_i=\beta_{XY,i}+X_{i-2}-\beta_{XY,i-2}-(X_{i-1}-\beta_{XY,i-1})\times F_i\left(...\right), \tag{24}$$

with coupling function term $\beta_{XY,i}$ leading to an additional shift with symmetry invariant

$$(X_i - \beta_{XY,i}) \cdot (X_{i-1} - \beta_{XY,i-1}) = (X_{i-1} - \beta_{XY,i-1}) \cdot (X_{i-2} - \beta_{XY,i-2}) = ... = C_X \ . \tag{25}$$

Reversely, the coupling from the X-system to the Y-system could be given symmetrically by

$$Y_i = \beta_{YX,i} + Y_{i-2} - \beta_{YX,i-2} - (Y_{i-1} - \beta_{YX,i-1}) \times F_i\,(...)\,, \tag{26}$$

with coupling shift $\beta_{YX,i}$ and symmetry invariant

$$(Y_i - \beta_{YX,i}) \cdot (Y_{i-1} - \beta_{YX,i-1}) = (Y_{i-1} - \beta_{YX,i-1}) \cdot (Y_{i-2} - \beta_{YX,i-2}) = ... = C_Y, \tag{27}$$

where the coupling has also 3 memory terms. As a result, we see for some special vector coupling functions $\beta_{XY,i}$ and $\beta_{YX,i}$ with radial distance dependent strength and scalar coupling constant c_3, e.g. by coupling two discrete paths by a symmetrical coupling function $\beta_{XY,i-1} = -\beta_{YX,i-1}$ with opposite signs and power-law exponent p_3

$$\beta_{XY,i-1} = c_3 \frac{X_{i-1} - Y_{i-1}}{|X_{i-1} - Y_{i-1}|^{p_3}} \ , \tag{28}$$

which can be extended two more than two coupled systems by superimposing the shifts of many mutual coupling functions. Two typical coupled system pattern are shown in Fig.5 and Fig.6. With the same control parameter the symmetry and scale between opposite "charges" can be broken by the expansion factor $c_4 \neq 1$ or with a different symmetry invariants $C_Y \gg C_X$ (scaling with radius, wave amplitudes or lengths, curvatures, or energies) depending on the initial conditions. The exponents leading to stable pattern are usually $p_3 = 2$ or $p_3 = 3$. Increasing the coupling, the spin axes change individually in some angular range (showing precession) until the chaotic range begins.

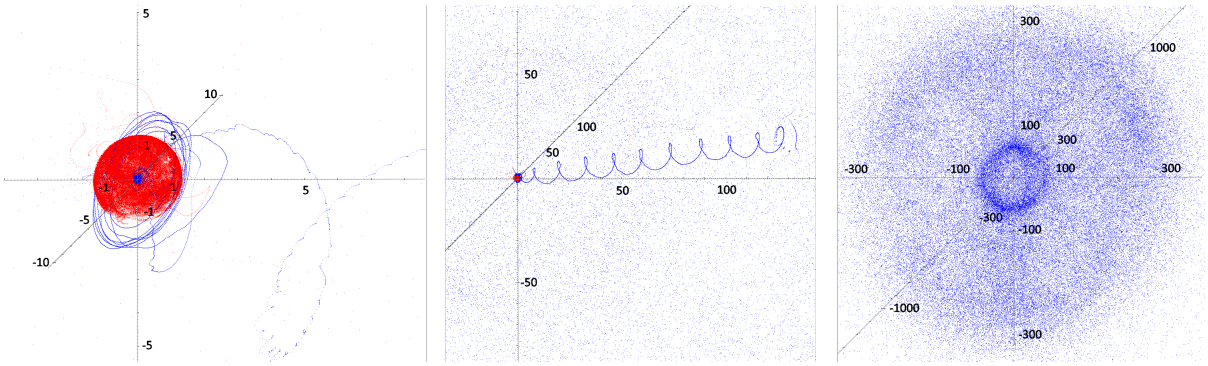

FIGURE 6. Two (blue, red) coupled type 1 quaternion systems with core region (left, highly enlarged), showing a helical packet emission from the core (mid, red core blue helix) transforming the local helical path into a non-local semi-stable kind of 2s-orbital cloud or wave (right, blue). The positive charge at the core in red (left) is surrounded by negative charges in blue (right). The neutral inner core (red and blue) is more than 2000 times smaller than the outer orbitals (blue), which have a size ratio about 1:4. We have $\beta_{XY,i} = -\beta_{YX,i}$, $\kappa \approx 0.0073\pi \approx \tau/\sqrt{3}$, $c_3 \approx -\pi/4$, $c_4 = 1.0$, $p_3 = 3$, $C_X \approx 0.00003808$, $C_Y \approx 1.0$, where the size difference is given by $C_Y \gg C_X$.

3.7. **Helical Paths.** The Frenet-Serret formulas are frequently used to describe the dynamics in multivariable space curves such as the helix in $\mathbb{R}^3$. Helical paths are curves of constant curvature κ and torsion τ and for which the tangent makes a constant angle $\theta = \arctan(\tau/\kappa)$ with a fixed line. General helices or Lancret curves appear in many applications, see Çiftçi [9]. In electromagnetism a charged particle in a static uniform magnetic field in Euclidean space $\mathbb{R}^3$ moves along a circular helix because of the Lorentz force (cross product between the velocity and magnetic field vector) and newtons equation. Lancret's theorem states that a necessary and sufficient condition for a curve to be a helix is that the ratio of curvature to torsion be constant. So it is not surprising that we find with our approach within the Frenet apparatus with type

1 $F_i(...)$ vector functions helical frame paths, especially in simulations with coupling showing spontaneous emission and absorption, see Fig.6. We often see a very interesting dynamics with $\sqrt{3}\kappa \approx \tau$ near to the helical angle $\theta = \pi/3 = \arctan(\sqrt{3})$. In Fig.6 we observe the characteristics of the helical emission, where the emitting core (in red) spins up an orbital state near to the core until (left picture) a critical spin is reached and the helical emission is started. The helical "spring" has often the same number of turns, the ratio pitch/diameter is related by the arctan of the helical angle to the ratio torsion/curvature.

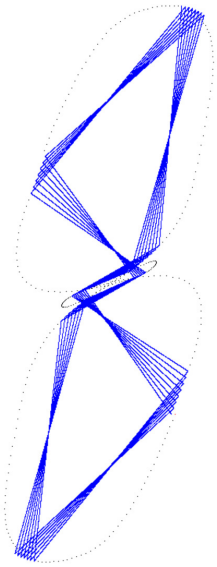

FIGURE 7. Split-octonion type 2 limit cycle structure on a twisted path with $N_2 = 8$ jumps per cycle $m = 8 \cdot 22 = 176$ fixed points, see Table 4, stable invariant, projected are 3 core dimensions out of $7d$. The blue rays show the " jump" structure.

4. Normed Algebras and Multiplication Tables

4.1. **Multiplication Tables.** How can we define and customize the algebra? Regarding orthogonality and normalization as the most important characteristics, the cross product is encoded in $n \times n$ (split-)multiplication tables, see Tables 2 and 3, where different table dimensions and classes characterize different algebras, see Hasebe [6] or Schray and Manogue [10]. The multiplication tables or tensors are known as the structure constants of the (split-)algebras. There is just one $3d$ cross multiplication table, but there are 480 versions of $7d$ cross algebra tables, so the cross operations in $7d$ have in contrast to the $3d$ cross operation not only 1 but 480 possible multiplication tables [10]. Although these different tables are all equivalent, a simulation or physical theory might make use of more than one multiplication table at any given time. In this context it should be noted, that we can define the $3d$ quaternion as a sub-algebra of the $7d$ octonion algebra, see Table 3. For practical reasons and as a interesting case, our simulation software can select for different coupled systems the algebra from different predefined multiplication tables. In our software, we can edit, switch to, and combine different algebras. We can even cut out an subset of operations. Our simulation software comes with some basic multiplication tables for all of this mentioned algebras as an validated input for computer experiments that can be modified.

4.2. **(split-)Octonion and (split-)Quarternion Algebra.** The cross product is usually defined by the algebra of pure imaginary quaternions ($n = 3$ imaginary components) part of octonions ($n = 7$ imaginary components), where the $7d$ cross product has the same relationship to the $8d$ (split-)octonions $\mathbb{O}$ as the $3d$ cross product does to the $4d$ (split-)quaternions $\mathbb{H}$ [6, 10]. The (split-)octonions correspond to the largest of the four normed algebras and are like the (split-)quarternions a division algebra over the real numbers,

TABLE 2. Example of a Split-octonion Multiplication Table, from [6].

1	e_1	e_2	e_3	e_4	e_5	e_6	e_7
e_1	-1	e_3	$-e_2$	$-e_5$	e_4	$-e_7$	e_6
e_2	$-e_3$	-1	e_1	$-e_6$	e_7	e_4	$-e_5$
e_3	e_2	$-e_1$	-1	$-e_7$	$-e_6$	e_5	e_4
e_4	e_5	e_6	e_7	1	e_1	e_2	e_3
e_5	$-e_4$	$-e_7$	e_6	$-e_1$	1	e_3	$-e_2$
e_6	e_7	$-e_4$	$-e_5$	$-e_2$	$-e_3$	1	e_1
e_7	$-e_6$	e_5	$-e_4$	$-e_3$	e_2	$-e_1$	1

TABLE 3. Structure of the Multiplication Table.

Table structure of a $7d$ algebra with a $3d$ sub-algebra	Encoding the split-octonion Table above

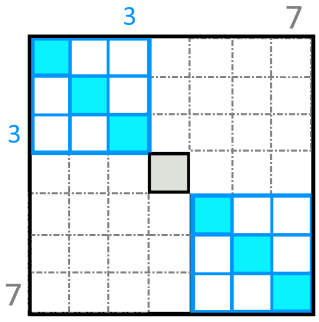


```
#DACOP 6.20--------------------
-1:No=3
00:L00=;+1;-1;-1;-1;+1;+1;+1;+1
01:L01=;+1;-1;+3;-2;-5;+4;-7;+6
02:L02=;+2;-3;-1;+1;-6;+7;+4;-5
03:L03=;+3;+2;-1;-1;-7;-6;+5;+4
04:L04=;+4;+5;+6;+7;+1;+1;+2;+3
05:L05=;+5;-4;-7;+6;-1;+1;+3;-2
06:L06=;+6;+7;-4;-5;-2;-3;+1;+1
07:L07=;+7;-6;+5;-4;-3;+2;-1;+1
08:TableClass=88s
09:Text=another split octonion
10:Ref=arXiv:0905.2792
11:Code=0123
```

a kind of hypercomplex number system. Split-octonions often show a very rich dynamics with limit cycles and subcycles, see Figs.7-9, where different frequencies can be observed, like a slow wave or orbit in some dimensions superimposed by a fast vibration or orbit in other dimension pairs.

4.3. **Signatures of (split-)Quaternions and (split-)Octonions.** A criterion is not only how many dimensions the algebra has, but also its signature - how many of these dimensions square to positive, negative or zero scalars. In Table 2 the signature of a split-octonion is located on the diagonal. This way we bring to life (split-)quaternions and (split-)octonions, which have different signatures, since in the splitted case not all dimensions square to negative. The split-algebras have the properties similar to the original division algebras except for their split signatures and provide for very important concepts [6]: few years after the discovery of quaternions by William R. Hamilton [11], James Cockle introduced the notion of the split-algebras [12, 13]. Similar to the original division algebras, there exist three species of split-algebras; split-complex numbers $\mathbb{C}'$, split-quaternions $\mathbb{H}'$, and split-octonions $\mathbb{O}'$. The Lagrangian for the classical superstring involves a relationship between vectors and spinors in Lorentz/Minkowski spacetime which holds only in 3, 4, 6, and 10 dimensions, these numbers are 2 more than the dimensions, see Baez [15] and Table 1 [6].

5. LIMIT CYCLES, MODULAR ARITHMETIC, AND EQUIVALENCE CLASSES

Limit cycles appear in all simulations depicted in this paper. Without limit cycles we would not observe the smoothness and arbitrary small shifts in closed loop discrete operations. Especially with split algebras we find nested sub-cycle structures, see Figs.8 and 9.

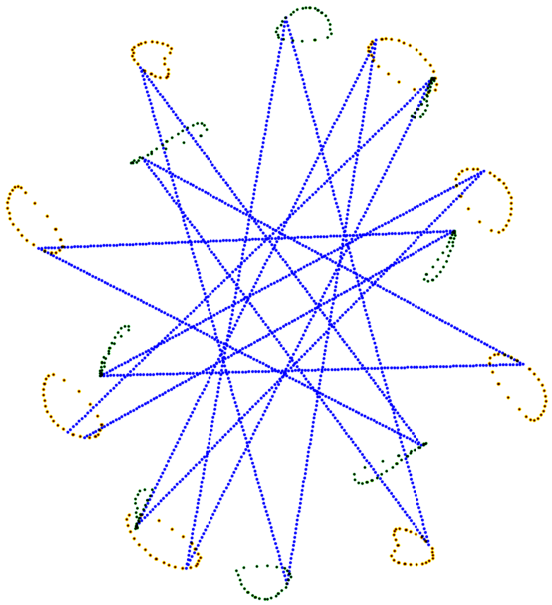

FIGURE 8. Scale-invariant split-octonion type 2 pattern with orbital limit cycle structure having 8 ring groups (yellow) including 8 reflection structures (green), each having $n = 26$ points, providing for a total limit cycle length $m = 416 = 2 \cdot 8 \cdot 26$. The violet lines show some "jump" paths connecting the group elements.

TABLE 4. Limit Cycle Split-Octonions with Sub-Cycles

Figure	b	N_1	N_2	N_3	$m = N_1N_2N_3$	$r = b - l$	m sphenic?
Fig.1	2	1	2	3	6	1	
	3	2	5	17	170	2	y
Fig.3	3	2	5	47	470	2	y
	3	2	8	17	272	2	n
Fig.8	3	2	8	26	416	2	n
	3	2	8	23	368	2	n
Fig.9	4	2	10	30	600	2	n
	5	2	17	27	918	2	n
Fig.4	4	3	7	59	1239	1	y
Fig.7	7	1	8	22	176	1	

5.1. **Nested Limit Cycles.** Given natural numbers $N_j \in \mathbb{Z}$, we can get spatial separated hierarchic N_j-gons, that are, closed sub-cyclic sequences, where the total cycle period is the product of the periods at every level j with maximum level J and

$$m = \prod_{j=1}^{J} N_j. \tag{29}$$

In other words, our system divides the total cycle into equivalence classes, each of the form $\{N_j = k_j b + r \mid k_j \in \mathbb{Z}\}$ where $r < b$. Here we have a modular arithmetic, where numbers N_j "wrap around" when reaching a certain value, called the modulus. The numbers N_j are equivalent if they have the same remainder when divided by some number b, a kind of hidden modular period. On a simple circular ring a cycle or sub-cycle with N_j elements does normally not correspond to angular segments with $2\pi/N_j$ angular units, since we have a modular or geometric shift l leading to $\pi \pm 2\pi/(N_j + l)$ units, where l is responsible for sub-cycle pattern generation, adding π is due to reflection, and $r = b - l < b$ is the remainder. The equivalence classes

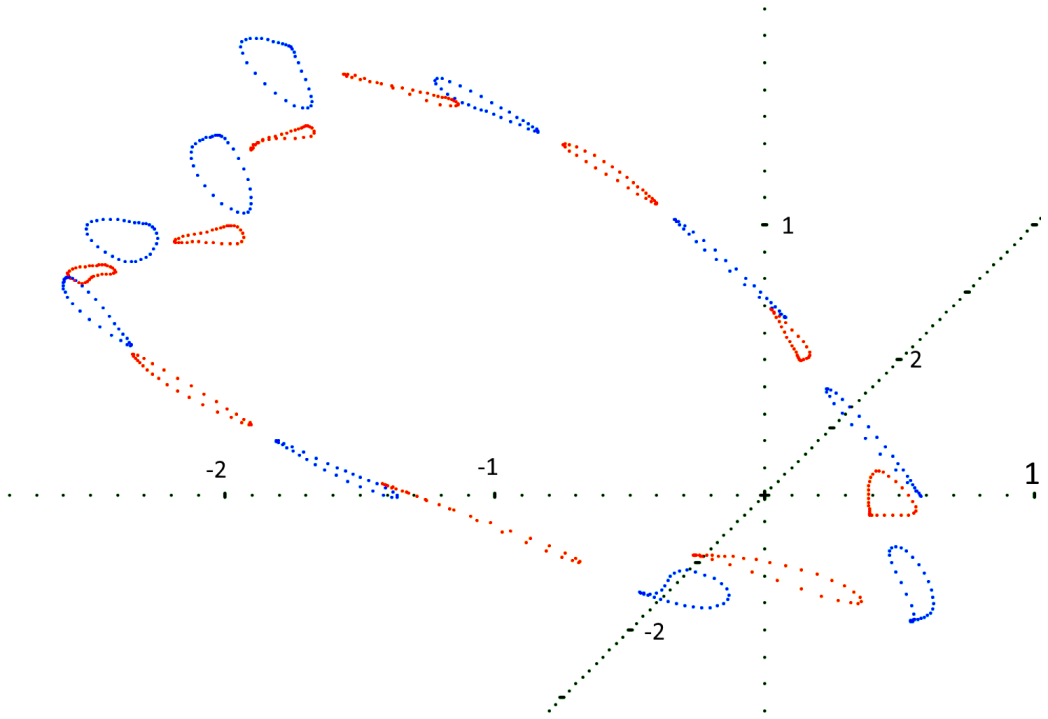

FIGURE 9. Type 2 split-octonion having orbital fixed point structure with 10 different ring groups and 10 reflection structures, each having 30 points, providing for a total limit cycle length $m = 600 = 2 \cdot 10 \cdot 30$. $c_1 \approx -0.1933$, $c_2 \approx 0.7839$, $p_1 = p_2 = 1$, $\alpha = 1$, C is not constant, so it is slightly instable.

are given by

$$N_i \equiv N_j \pmod{b}, \tag{30}$$

where b divides $N_i - N_j$, or N_i and N_j have the same remainder r when divided by b, which holds for $N_j = k_j b - l$ (or $N_j = b^j - l$).
The emergence of sub-cycles happens especially in type 2 split-octonions, where we always have $J = 3$, which means that m is a sphenic number if all three N_j are prime. Examples are given in Table 4 and especially in Fig.8 with visible jump paths, where $m = 2 \cdot 8 \cdot 26 = 416$. Here we have $N_j = b^j - l$ elements for $j = 1, 2, 3$ and $l = b - r$ with base $b = 3$ and remainder $r = 2$ giving $l = b - r = 1$. Our simulations suggests that with our approach $m = 4$ and $m = 6$ are the smallest stable limit cycles. As another result from Table 4, m is always the product of three equivalent numbers N_j.

6. Sharp Tangential - Radial Modal Transition

Both of our two proposed Frenet type vector functions show some interesting spin dynamics in $3d$ and $7d$. We found very interesting transition with hysteresis for special values of α, κ, τ. With a type 1 or 2 vector function, a unit curvature $\kappa = 1$, unit scale $C = 1$ on the sphere, a small coupling constant α (velocity parameter , see Eq.(13), and a torsion parameter $\tau \approx \sqrt{3}\kappa$, we get a simple $1d$ ring pattern. Increasing the ratio κ/τ or c_2/c_1 slightly, some $2d$ off-equatorial spherical surface pattern appear, see Fig.10. Without spiral we have Viviani's curve (looks like an infinity symbol on the sphere, cylinder intersecting a sphere) as a generalized helical curve, which can also be found in simulations. Finally, the tangential motion turns spontaneously within a very small range of the ratio into a $3d$ radial helical motion with cylindrical structures, see Fig.11. More in detail, the binormal component stimulates off-equatorial patterns, which often look like

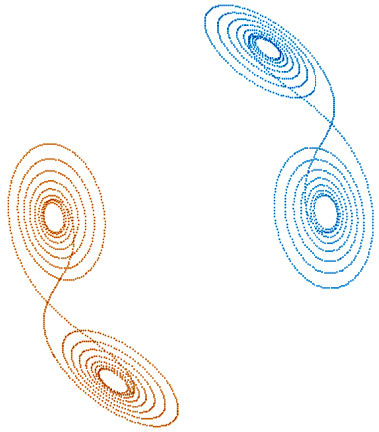

FIGURE 10. $3d$ A scale-invariant type 2 quaternion pair, point symmetric, perfectly stable, pure angular modes on the sphere with constant radius and constant $C = 1$, can run under $7d$ split and non-split without change. $c_1 \approx -0.0073$, $c_2 \approx -\sqrt{3}c_1$, $p_1 = p_2 = 1$, $\alpha = 1$.

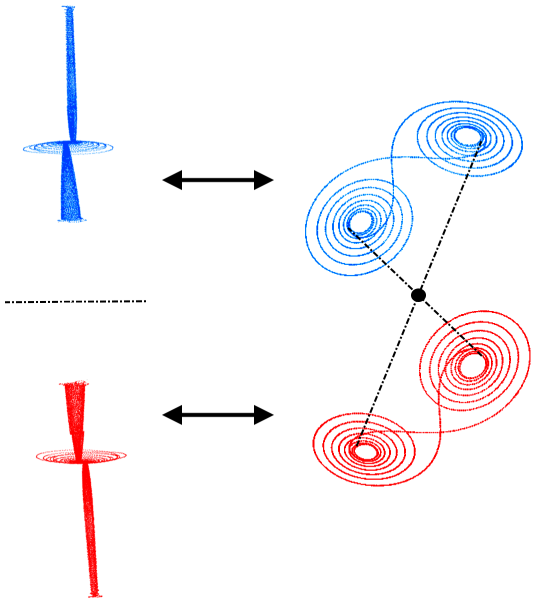

FIGURE 11. A scale-invariant type 2 quaternion pair with excited radial modes from Fig.10. The pair shows a modal transition between mirror symmetric radial (left) and point symmetric orbital modes (right). The modal transition with hysteresis happens in a very small torsion range ($\Delta\tau/\tau < 10^{-7}$), see Table 5. $p_1 = p_2 = 1$.

the infinity symbol ∞ with some extra loops, as long as in Eq.(18) the curvature/torsion ratio

$$g_a = -\sqrt{3}c_2/c_1 \tag{31}$$

is below a critical threshold. Increasing g_a we find at some ratio g_{a_2} (where the orbital angular range collapses) that radial modes or vibrations get excited. It seems, that one of two orbital modes in Fig.10 collapses into a radial oscillation with a thin helical or cylindrical shape, see Fig.11.

Comparing the orbital structures of a type 1 with a type 2 vector function, there are some differences regarding the excitation of radial modes. Increasing g_a, the type 2 transition to radial modes occurs spontaneously

TABLE 5. Sharp normal-tangential type 2 phase transition between $g_{a_1}...g_{a_2}$, where $C = 1$

α^{-1}	$g_{a_1} = -\sqrt{3}c_2/c_1 \approx 1 + \frac{\alpha}{2\pi}$	g_{a_2}	$(g_{a_2} - g_{a_1})/g_{a_1}$	$2\alpha^{-2}\frac{g_{a_2}-g_{a_1}}{g_{a_1}+g_{a_2}-2}$
20	1.008959597	1.008959938	3.37756E-07	0.015213901
100	1.001601099	1.001601168	6.9307E-08	0.433554973
137.0359996	**1.001159968**	1.001160029	6.09683E-08	0.988141622
137.7	1.001154267	1.001154328	6.0802E-08	**0.999929527**
200	1.000789955	1.000790003	4.7300E-08	2.396894339
1000	1.0001563375	1.0001563486	1.1134E-08	71.2280004

above a special threshold value g_{a_2} in contrast to type 1. Decreasing the ratio back to lower values we find hysteresis, where the radial mode reverts back to a spherical mode for $g_{a_1} < g_{a_2}$. We find that g_{a_1}, g_{a_2}, $g_{a_1} - g_{a_2}$ depend on the velocity or coupling constant α, the stronger the coupling, the higher the anomaly g_a. Regarding the values that are listed in Table 5, there is a similarity to the anomaly in the electron g-factor ($g_e = 2 \cdot 1.00115965218...$, see Fan et al. [14], since we also find $g_a \approx 1 + \frac{\alpha}{2\pi}$ and approximately $g_e = 2g_a = -2\sqrt{3}c_2/c_1 \approx 2 + \frac{\alpha}{\pi}$, which was calculated as the first correction term by quantum electrodynamics long ago. Therefore, it is plausible also to take for a test the fine structure constant as an electromagnetic coupling constant α, see Table 5. $\sqrt{3}$ is the long diagonal between opposite corners in the $3d$ unit cube, $2\sqrt{3}$ is the normalizing distance of reflection, the distance of a point to its reflected point from flipping the sign of all three orthogonal unit vectors (normal, tangential, binormal).

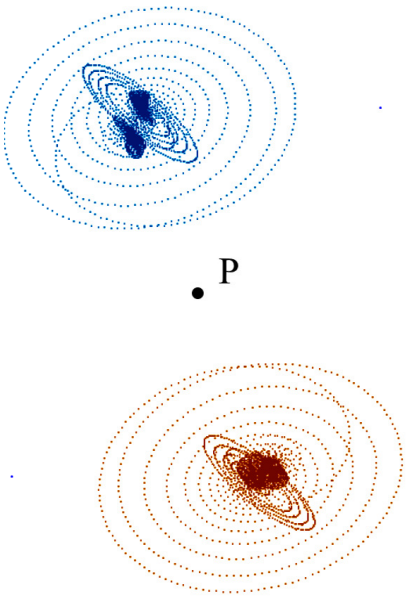

FIGURE 12. A scale-invariant type 2 octonion pair acting in $7d$ with more than 3 modes excited (radial and orbital modes simultaneously). This is the octonion version of the quaternion pair in Fig.10. It is also point symmetric to P, perfectly stable with constant $C = 1$, has the same parameter like the quaternion in Fig.10, but shows no sharp transition between modes. $c_1 \approx -0.0073$, $c_2 \approx -\sqrt{3}c_1$, $p_1 = p_2 = 1$, $\alpha = 1$

Here we can also see a difference between type 1 and type 2 vector functions. In contrast to type 1, the type 2 sequences shows by varying the torsion parameter a very sharp transition $\Delta\tau/\tau < 10^{-7}$ from spherical to radial modes and vice versa while showing hysteresis loop if we vary torsion or curvature up and down. Note, that the mirror symmetry changes to a point symmetry and vice versa, see Figs.10 and 11. Hysteresis is the dependence of the state of a system on its history and can therefore be attributed to the memory terms in our non-linear system. Geometrically, the new oscillation is orthogonal to an existing

oscillation (with memory = conservation of spin) stating a new imaginary dimension forcing a rotation in a new imaginary plane. This process excites harmonics, waves, and rotations in all possible orthogonal degrees of freedom. To stimulate another orthogonal mode or rotation, the new degree of freedom must be in concert (orthogonal and in phase) with existing degrees of freedom. Such a behavior showing a phase transition while exciting an extra dimension can be found in simulations. Hysteresis means, that there is not only memory or entropy/information stored in the system but also some power buffered, where the system could act on the hysteresis cycle like a pump. The last column in Table 5 compares the relative hysteresis power $(g_{a_2} - g_{a_1}/(g_{a_1} + g_{a_2} - 2)$ with the coupling power $\alpha^2/2$, and it turns out that both have similar values at $\alpha^{-1} \approx 137$ with hysteresis range $g_{a_2} - g_{a_1} \approx \alpha^3/(2\pi)$. Regarding this number and basic meaning of hysteresis regarding storage and coupling of energy, the hysteresis could be crucial in coupling different system connected in a radial direction, where modes get excited with enough hysteresis power and coupling strength.

7. Conclusions

Bringing the (split-)quaternion and (split-)octonion system to life by orthogonal components in a time-discrete recurrent frame, we change the normal component by tangential and binormal components generating the next frame. The non-linear recurrent model of kinematic curve generation results in complex paths of orbital and radial modes. Even on simple tangent paths on spherical surfaces with constant curvature there are nonlinear geometric effects on the orbital path. We find two related vector functions driving the frame path by tangential and binormal components, where type 2 is scale-invariant for $p_1 = p_2 = 1$. Different normed algebras in $3d$ and $7d$ can be applied to get the orthogonality and related symmetry. The two main symmetries are given by the reflection mirror symmetry and the invariant C. Monitoring C shows if a pattern is stable or not, since stability and a stable limit cycle requires special values of torsion and curvature with proper initial conditions. Limit cycle modular arithmetic with equivalence classes characterizes the resulting point groups, rings, or N_j-gons. We could split a limit cycle into sub-cycles with level $1 \leq j \leq J = 3$, where we find a limit cycle number $m = N_1 N_2 N_3$ as a the product of three numbers N_j. If all N_j with $J = 3$ are prime, m is a sphenic number.

Very interesting regarding further computer experiments and vector functions are the transitions between orbital and radial modes. Here we see, which fundamental aspects of our approach are relevant for a sharp transition as a resonance with hysteresis, which can in our case only be found with three degrees of freedom. We find, that the transition usually occurs at a special helical angle condition near to $\theta = \arctan(\tau/\kappa) = \arctan(\sqrt{3}) = \pi/3$. During the orbital/radial transition the orbital mode transforms in radial direction into a helical path. Coupling two systems is supported by this transition, eventually a new approach to the well-known anomalous g-factor of an interacting positron-electron pair. With a spherical symmetry the radial coupling strength is a $p_3 = 3$ power-law, resulting in helical emissions resembling a charged particle moving radially in a magnetic field. After the helical path has reached a critical length or radial distance, it transforms into a non-local bound state of an orbital cloud around a very tiny core.

The recurrent operations approach could be interesting in all fields the algebras already have been applied, which are Clifford algebras and spinors, projective geometry with Hopf fibrations and Lorentzian geometry, Jordan algebras, and the exceptional Lie groups - and there are many applications in quantum physics and relativity. The existence of classical supersymmetric string theories has been linked to the existence of the normed division algebras [10], see Table 1. Since relativistic quantum physics (Dirac) can be formulated by this algebra, see e.g. [15, 16], and the Frenet frame approach directly shows the geometric role of torsion and curvature in the context of electromagnetism, we could try to link to quantum and relativistic physics and eventually identify some interesting real existing orbital wave solutions that could be relevant in this context. The concept of long-range reflection jumps introduces a kind of non-locality, which is important in the context of quantum physics. But there are also local helical paths starting at a core and forming a bound state surrounding the core. Curvature and torsion properties have already be related to electromagnetic fields. The spin/curvature anomaly found in the context of a radial mode excitation threshold with hysteresis could be a good starting point. Geometric shifts induced by parallel transport can be related to the surface curvature and torsion, where extra angles or angular shifts are responsible for pattern generation. Building

this way complex structures, modular arithmetic gives the extra angles and geometric shifts on closed, discrete, and curved paths. This relation is still open.

In future works we will consider not only one isolated system with one algebra, we will apply different algebras in parallel, where we can modify, couple or split algebras in variable multiplication tables. But this approach requires more understanding and improvement of the simulation methods. There are still a lot of interesting open points, some of which will be clarified sooner or later. Videos from simulations can be found on the internet with the tag #DACOP.

References

[1] Binder, B. (2022), Dynamic Localized Autonomous Chaotic Orbital Patterns from Rotation-Translation Sequences, *Springer Proceedings in Complexity*, **14th** Chaotic Modeling and Simulation International Conference, Springer Nature, 45–54.

[2] Skiadas, C.H. (2009), Von Karman Streets Chaotic Simulation, *Topics on Chaotic Systems*, World Scientific, 309-313.

[3] Binder, B. (2022), Orbital Waves and Quantum Densities from Time-Discrete Chaotic Sequences, *Springer Proceedings in Complexity*, **15th** Chaotic Modeling and Simulation International Conference, Springer Nature, 29-40.

[4] Binder, B. (2024), Time-Discrete SO(3) Jump Sequences Showing a Quantum Type Orbital Wave Dynamics, presentation in: *Days Of Applied Nonlinearity and Complexity (DANOC)*, Book of Abstracts, January 12-14.

[5] Hurwitz, A. (1898), Ueber die Composition der quadratischen Formen von beliebig vielen Variabeln (On the composition of quadratic forms of arbitrary many variables) (in German). *Nachr. Ges. Wiss. Göttingen*, 309-316.

[6] Hasebe, K. (2010), The split-algebras and non-compact Hopf maps, *J. Math. Phys.* **51**(5):053524-053524-35.

[7] Hu, S., Lundgren, M. and Niem, A. J. (2011), Discrete Frenet frame, inflection point solitons, and curve visualization with applications to folded proteins, *Phys. Rev.* **E 83**, 061908.

[8] Blair, D. E. and Konno, T. (2011), Discrete torsion and its application for a generalized van der Waerden's theorem, *Proc. Japan Acad.*, **87**, Ser. A, No.10, 209-214.

[9] Ciftci, Ü. (2009), A generalization of Lancret's theorem, *Journal of Geometry and Physics*, **59**, 1597–1603.

[10] Schray, J. and Manogue, C. A. (1996), Octonionic representations of Clifford algebras and triality, *Foundations of Physics.* **26**, 17–70.

[11] Hamilton, W. R. (1844), On a new Species of Imaginary Quantities connected with a theory of Quaternions, *Proceedings of the Royal Irish Academy*, **2**, pp. 424-434.

[12] Cockle, J. (1848), On Certain Functions Resembling Quaternions, and on a New Imaginary Algebra, *Phil. Mag.* **(3) 33**, 435-439.

[13] Cockle, J. (1849), On a New Imaginary in Algebra, *Phil. Mag.* **(3) 34**, 37-47. On Systems of Algebra Involving more than one Imaginary and on Equations of the Fifth Degree, *Phil. Mag.* **(3) 35**, 434-437.

[14] Fan, X., Myers, T. G., Sukra, B. A. D. and Gabrielse, G. (2023), Measurement of the Electron Magnetic Moment. *Physical Review Letters.* **130** (7).

[15] Baez, J. (2002), The Octonions, *Bull. Amer. Math. Soc.* **39** (2): 145-205.

[16] Shapiro, D. B. (2000), *Compositions of Quadratic Forms*, W. de Gruyter Verlag.

Acknowledgements

I would like to acknowledge André E. Botha for helpful discussions about this work.